Characterization of the cellular response triggered by gold nanoparticle–mediated laser manipulation

Stefan Kalies
Sebastian Keil
Sina Sender
Susanne C. Hammer
Georgios C. Antonopoulos
Markus Schomaker
Tammo Ripken
Hugo Murua Escobar
Heiko Meyer
Dag Heinemann

Characterization of the cellular response triggered by gold nanoparticle–mediated laser manipulation

Stefan Kalies,[a,*] Sebastian Keil,[a] Sina Sender,[a] Susanne C. Hammer,[b,c] Georgios C. Antonopoulos,[a] Markus Schomaker,[a] Tammo Ripken,[a] Hugo Murua Escobar,[b,c] Heiko Meyer,[a] and Dag Heinemann[a]
[a]Laser Zentrum Hannover e.V., Department of Biomedical Optics, Hollerithallee 8, Hannover 30419, Germany
[b]University of Veterinary Medicine, Small Animal Clinic, Bünteweg 9, Hannover 30599, Germany
[c]University of Rostock, Department of Hematology, Oncology, and Palliative Medicine, Ernst-Heydemann-Street 6, Rostock 18057, Germany

Abstract. Laser-based transfection techniques have proven high applicability in several cell biologic applications. The delivery of different molecules using these techniques has been extensively investigated. In particular, new high-throughput approaches such as gold nanoparticle–mediated laser transfection allow efficient delivery of antisense molecules or proteins into cells preserving high cell viabilities. However, the cellular response to the perforation procedure is not well understood. We herein analyzed the perforation kinetics of single cells during resonant gold nanoparticle–mediated laser manipulation with an 850-ps laser system at a wavelength of 532 nm. Inflow velocity of propidium iodide into manipulated cells reached a maximum within a few seconds. Experiments based on the inflow of FM4-64 indicated that the membrane remains permeable for a few minutes for small molecules. To further characterize the cellular response postmanipulation, we analyzed levels of oxidative heat or general stress. Although we observed an increased formation of reactive oxygen species by an increase of dichlorofluorescein fluorescence, heat shock protein 70 was not upregulated in laser-treated cells. Additionally, no evidence of stress granule formation was visible by immunofluorescence staining. The data provided in this study help to identify the cellular reactions to gold nanoparticle–mediated laser manipulation.
© *2015 Society of Photo-Optical Instrumentation Engineers (SPIE)* [DOI: 10.1117/1.JBO.20.11.115005]

1 Introduction

Laser transfection has proven to be an enabling technology in cell biology allowing alternative development of regenerative approaches. The specific features of laser transfection, which combines high efficiency, minimal invasive treatment of the cells, and spatial selectivity, fulfill key requirements for directed cell manipulation.[1–3]

Early demonstration of laser-induced membrane permeabilization using a membrane-targeted 355 nm Nd:YAG laser with a pulse length of 5 ns in normal rat kidney cells was realized as early as 1984.[1] The following studies focused on the improvement of this application using similar laser parameters.[4,5] Additionally, the combination of continuous wave irradiation with the absorption of phenol red in the cell culture medium for dye-assisted laser-induced membrane permeabilization or the laser-based transfection of plant cells was investigated.[6,7] A seminal achievement in the field was realized by the introduction of femtosecond laser pulses for targeted single-cell laser transfection leading to extremely high DNA transfection efficiencies.[2] Femtosecond single-cell laser transfection is reviewed in detail by Stevenson et al.[3] Further, several experimental settings based on femtosecond laser transfection were evaluated, including the application of femtosecond laser pulses via endoscopic systems, the use of a spatial light modulator to specifically target cells, or microfluidic platforms to enhance the throughput of the method.[8–10]

Although single-cell laser transfection is well suited to follow individual cells' fates after transfection, the technique does not allow to transfect a high cell number in reasonably short time scales. However, high efficiencies are required in high-throughput screening of pharmaceutically or therapeutically active compounds or to manipulate high cell numbers for cell reconstructive therapies.[11] Several groups evaluated multicell laser perforation setups using the emission of a laser-induced stress wave for cell membrane permeabilization.[12–14] These approaches were extended resulting in actual gene transfection *in vivo*.[15,16] Recently, Wu et al.[17] introduced a silicon array containing small holes and channels providing a pressurized flow during the laser transfection procedure. Titanium films at the sides of each hole are heated by a scanning nanosecond laser beam triggering cavitation bubbles for membrane permeabilization. This approach enabled the delivery of proteins, nanoparticles, and bacteria into cells.[17] A third approach uses membrane adhered gold nanoparticles irradiated by weakly focused laser pulses. Thereby, high cell numbers can be treated rapidly. Typically, either resonant (around 532 nm) or off-resonant (around 800 nm) excitation of the gold nanoparticles is applied using laser pulse length ranging from femto- to nanoseconds. Boulais et al.[18] recently reviewed the physical mechanism of this permeabilization procedure in detail. Heating of the particles or near-field enhancement of the particles can lead to bubble formation, finally causing membrane perforation.[18,19] Several recent studies studied the efficiency of DNA, siRNA, Morpholino, and protein delivery and cell viability after treatment using this method. Thereby, various laser parameters, including resonant and off-resonant irradiation of the gold nanoparticles, were taken into account.[20–24] However, the biological consequences of this approach and

other laser transfection procedures are still not well understood. Addressing this, we previously analyzed cell membrane potential changes by patch clamp analysis in off-resonant gold nanoparticle–mediated laser transfection.[25] Furthermore, we analyzed the dependence of dextran inflow into the cells on the extracellular salt concentration and observed no dependency on the osmolarity.[26] Additionally, we showed that dextrans up to 2000 kDa can pass the cell membrane during the perforation procedure.[26] Recently, we were able to provide a comprehensive analysis of four important cell parameters: cell volume and area, ion exchange (calcium), and the cytoskeleton (filamentous actin) in resonant gold nanoparticle–mediated laser manipulation with 850 ps laser pulses by a multimodal imaging setup.[27] Despite these analyses, an exhaustive characterization of the transfection procedure requires an extension of this work to the perforation kinetics and oxidative or heat-induced cell stress phenomena. A detailed examination of these additional parameters was performed within this study and extends the biophysical and biochemical analysis of the cell response in laser transfection. We analyze the perforation procedure by propidium iodide and FM4-64 inflow, detect the increased formation of the reactive oxygen species (ROS) via a dichlorofluorescein-based assay, evaluate heat stress by quantitative real-time polymerase chain reaction (PCR) marker gene analysis, and investigate the formation of stress granules by antibody staining.

2 Methods

2.1 Laser Manipulation Setup

Two different manipulation systems, employing the same laser source, were used in this study to investigate the cellular response triggered by gold nanoparticle–mediated laser manipulation. The laser source is an 850-ps laser system operating at a wavelength of 532 nm and a repetition rate of 20.25 kHz (Horus, France).

Our microscopy setup allows following the treatment of a few cells in glass-bottom dishes by a multimodal imaging approach. In this study, we used the fluorescence imaging part of this setup as described by us previously.[27] It is based on epifluorescence illumination with a mercury vapor lamp. Fluorescence images were recorded with a CCD camera (Progres MF Cool, Jenoptik, Germany). An OD6 notch filter (NF533-17, Thorlabs, Germany) was employed to attenuate the manipulation beam. Cells were randomly selected using a motorized stage with bright field illumination. A fixed irradiation time of 40 ms was applied for manipulation. The parameter space was based on our previous study with three radiant exposures covering the threshold of perforation (15 mJ/cm^2), high perforation efficiencies and good viability (27 mJ/cm^2), and invasive treatment of the cell, possibly leading to cell death (41 mJ/cm^2).[27] Moreover, light scattering of gold nanoparticles was detected using a 535 nm $\pm$ 20 nm excitation filter and a 520 nm longpass emission filter.

Our high-throughput setup was used in previous studies to treat and analyze the efficiency of molecular delivery (siRNA, Morpholinos, and proteins) and the cell viability of high cell numbers.[21,24,28] A single well of a 96-well plate can be handled within 8 s and examined afterward in a separate fluorescence microscope. In this study, two scanning velocities were applied. The standard perforation procedure irradiates cells with a radiant exposure of 42 mJ/cm^2 and a scanning velocity of 200 mm/s. Invasive treatment of the cells is accomplished by

reducing the scanning speed to 50 mm/s.[21,26] Although both irradiation times (scanning velocities) are shorter than the irradiation time of the microscopic setup, the parameter regimes are comparable.[21,27]

2.2 Cell Culture and Nanoparticle Labeling

Canine ZMTH3 cells were used in all experiments, except for the immunofluorescence staining of T-cell internal antigen-1 related (TIAR) protein in murine L929 cells owing to the antibody species specificity. Each cell line was cultured in RPMI 1640 medium supplemented with 10% of fetal bovine serum and 1% of the antibiotic Zellshield (all Biochrom, Germany). Spherical gold nanoparticles of 200 nm diameter (PGO200, Kisker, Germany) were added 3 h before perforation at concentrations of 0.05 and 0.5 μg/cm^2. The first concentration was used in the perforation kinetics and oxidative stress measurements to investigate the perforation with a minimal number of particles ($\sim$5) per cell. The latter concentration of 0.5 μg/cm^2 is equivalent to $\sim$30 particles per cell in a glass-bottom dish. This parameter is routinely used in gold nanoparticle–mediated laser transfection.[21]

2.3 Analysis of Perforation Kinetics

Analysis of perforation kinetics was performed in the microscopy setup in glass-bottom dishes (μ-Dish 35 mm, ibidi, Germany) with 150,000 ZMTH3 cells seeded 24 h prior to the experiment. To analyze the propidium iodide inflow, 1.5 μM propidium iodide (Life Technologies) was added to the cell medium. Propidium iodide, a membrane impermeable dye with a molecular weight of 670 Da, becomes fluorescently detectable upon binding to nucleic acids after inflow. This molecule is extremely small compared to the cell, enabling isotropic inflow at the site of perforation. Within the cytoplasm, propidium iodide immediately binds nucleic acids, limiting the concentration of free propidium iodide to nearly zero. The change of the fluorescent area over time indicates the diffusion of propidium iodide–nucleic acid complexes from the perforation site.[29] The diffusion is dominated by the nucleic acids, which are larger and heavier than propidium iodide.[29] The respective area was outlined in ImageJ and analyzed based on a custom-written ImageJ macro for threshold analysis.[30] Within a few minutes, propidium iodide might pass into the cell nucleus and stain it brightly owing to the high concentration of nucleic acids compared to the cytoplasm. This would exacerbate the analysis on a longer time scale. As a consequence, to examine the behavior on a minute time scale, we switched to the dye FM4-64 (Life Technologies) that was previously used in membrane repair analysis.[31] This dye binds the outer leaflet of the membrane and penetrates the cell after perforation. We measured the change of fluorescence per cell, which should saturate with membrane repair. Cells were outlined in ImageJ, fluorescence was measured, and a background fluorescence value was subtracted for each image of a stack. A concentration of 1 μg/ml FM4-64 was applied. FM4-64 and propidium iodide fluorescence were excited using a 535 nm $\pm$ 20 nm bandpass filter and detected with a 610 nm $\pm$ 25 nm filter. All data points show the mean and standard error of five single cells in three independent samples.

2.4 Quantification of Oxidative Stress

The examination of the increased formation of ROS was performed using the microscopic setup in glass-bottom dishes

with 150,000 seeded ZMTH3 cells. Carboxy-H$_2$DCFDA (Life Technologies) was added to the cell medium at a working concentration of 25 μM in HEPES buffered saline (25 mM HEPES, 120 mM NaCl, 5.4 mM KCl, 1.8 mM CaCl$_2$, 25 mM NaHCO$_3$, and 15 mM glucose, pH 7.4). The cells were incubated for 30 min at 37°C and washed with HEPES-buffered saline afterward. Acetate groups are removed by intracellular esterases, and upon oxidation by ROS, the fluorescent product dichlorofluorescein (DCF) is yielded. A control group (only laser irradiated, without gold nanoparticles) accounting for photobleaching effects was also analyzed. DCF fluorescence was excited using a 480 nm $\pm$ 15 nm bandpass filter and detected with a 520 nm longpass filter. Image analysis was performed according to the Sec. 2.3 All data points represent the mean and standard error of five single cells in three independent samples.

2.5 Quantification of Heat Stress

For quantitative PCR (qPCR) analysis, 100,000 ZMTH3 cells were seeded per well in a 24-well plate, and three wells were pooled per sample after laser treatment in the high-throughput setup. RNA expression of the heat inducible stress marker gene heat shock protein 70 (HSP70) relative to the housekeeping genes beta-actin (ACTB) and glyceraldehyde 3-phosphate dehydrogenase (GAPDH) was analyzed 2 h after laser or heat treatment (30 min at 45°C) via quantitative reverse transcription PCR (RT-qPCR) analysis. RNA was purified with a phenol/chloroform-based protocol using the commercially available reagent TriFast (peqlab, Germany). DNAseI (RQ1 DNase, Promega, Germany) treatment of purified RNA was performed to ensure complete removal of remaining genomic DNA. 25 ng of RNA was used for quantification and mixed with SYBR green (QuantiTect SYBR Green RT-PCR, Qiagen, Germany), canine HSP70 primers (PPF00191A, Qiagen), and reverse transcriptase. Expression of HSP70 was quantified relative to the housekeeping genes ACTB and GAPDH and comparatively normalized to the untreated sample. The expression analyses were performed using the Mastercycler realplex (Eppendorf AG, Germany). RT-qPCR conditions were 30 min at 50°C and 15 min at 95°C, followed by 40 cycles with 15 s at 94°C, 30 s at 58.5°C, and 30 s at 72°C. Gene expression levels were derived based on the $\Delta\Delta CT$ method, and statistical analysis was done using the software tool REST 2009.[32] A p value of ≤ 0.05 was considered statistically significant.

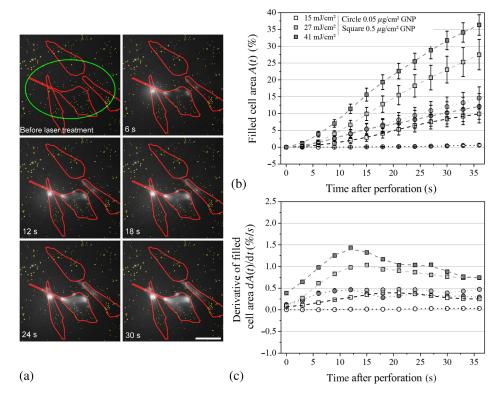## 2.6 Immunofluorescence Staining of T-Cell Internal Antigen-1 Related Protein

Antibody staining of stress granules (TIAR protein) was performed in black, clear-bottom 96-well microplates with 30,000 seeded L929 cells in the high-throughput setup. After laser treatment, cells were briefly washed with phosphate-buffered saline (PBS), fixed with 4% of paraformaldehyde in PBS (Sigma Aldrich, Germany), and permeabilized with 1% Triton-X 100 in PBS (Sigma Aldrich). Two washing steps with 3% bovine serum albumin (BSA) plus 0.05% Tween 20 in PBS were followed. Incubation for 45 min in 10% goat serum in PBS served to block unspecific binding. The primary antibody (TIAR D32D3 XP Rabbit mAb, NEB, Germany) was diluted 1:1000 and added to the cells in 3% BSA in PBS over night at 4°C. Two washing steps in 3% BSA plus 0.05% Tween 20 in PBS were followed. The secondary antibody [Goat anti-

Rabbit IgG H&L (Alexa Fluor 488), abcam) was diluted 1:500 in 3% BSA in PBS and added to the cells for 1 h at room temperature. Finally, cells were washed three times with PBS, and cell nuclei were costained with 9 μM Hoechst 33342 (Life Technologies). Subsequently, cells were imaged using a fluorescence microscope (Zeiss Axiovert 200, Carl Zeiss, Germany) equipped with an EMCCD-camera (Andor Luca R, Andor).
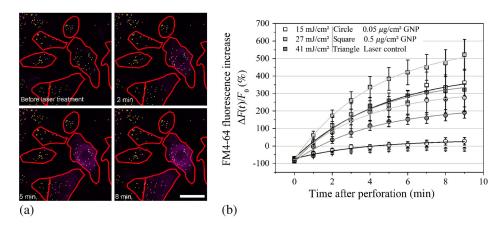
3 Results and Discussion

3.1 Investigation of Perforation Kinetics During Gold Nanoparticle–Mediated Laser Manipulation

A key issue of molecular delivery is the actual achieved inflow of molecules during perforation. In laser-induced perforation, the solute transport is dominated by simple diffusion, while large structures, such as plasmids, might enter the cell through membrane adherence after perforation.[33] The kinetics of the perforation procedure acting hereby is currently still unknown. We investigated the inflow of propidium iodide during the first few seconds after perforation in this study [see Figs. 1(a) and 1(b) and Video 1], based on our previous work.[27] In detail, we determined the area of the cell in which propidium iodide–nucleic acid complexes have diffused after perforation, normalized to the total cell area. We observed that not all irradiated particles contributed to the inflow of propidium iodide. The interaction of laser light and particles is possibly affected by the position of the particles relative to the intensity profile of the laser. Additionally, optical properties of the particle could be altered owing to the formation of a soft protein corona around the particle combined with the beginning of endocytotic uptake.[34] Protein–particle complex building might change the absorption of the laser light. A laser radiant exposure of 15 mJ/cm^2 is the threshold of perforation and led to the lowest inflow of propidium iodide after perforation [see Fig. 1(b)]. The highest achieved inflow of propidium iodide was observed in the damage regime of the cells upon applying a radiant exposure of 41 mJ/cm^2. Two effects could contribute to these observations: a higher radiant exposure leading to more pronounced heating and associated bubble formation at the particles,[18] additionally, as mentioned above, higher radiant exposures might induce perforation at particular particles that are affected by the environment or by their position relative to the laser spot.

To examine the kinetics of perforation during the first few seconds after laser treatment, we calculated the first derivative of the filled area per time, which constitutes a velocity of area inflow per time [see Fig. 1(c)]. Interestingly, the highest velocity was observed ~10 s after perforation, in particular in the damage regime of 41 mJ/cm^2. This observation matches results of our previous study using digital holography to analyze the volume outflow during perforation, where we observed two phases of volume exchange. The fast phase volume outflow occurred during the first 10 s accompanied by a lower, linear outflow of volume in the following time.[27] Based on these combined study results, it is reasonable to assume a sequential-steps perforation procedure. Schomaker et al. performed patch clamp analysis and observed multiphase behavior with a rapid inflow of ions in 6 to 10 s followed by a smaller increase of current.[25] Furthermore, the cellular calcium response also occurs in the first few seconds after perforation in gold nanoparticle–mediated laser manipulation, resembling a rapid inflow of ions.[27] Consequently, we can assume that this first phase of perforation

(a)

(b)

(c)

Fig. 1 Inflow of propidium iodide and area covered by propidium iodide–nucleic acid complexes in ZMTH3 cells during the first few seconds after gold nanoparticle-mediated laser manipulation. (a) Sequence of contrast-enhanced images from Video 1 after the perforation event showing the inflow at single particles. Inflow does not occur at all irradiated particles. A radiant exposure of 27 mJ/cm^2 and a concentration of 0.5 μg/cm^2 gold nanoparticles were applied. Cells are outlined red, and gold nanoparticles are depicted in yellow. Laser spot is outlined in green. Scale bar: 20 μm. (b) The area in which propidium iodide diffuses is dependent on laser radiant exposure and nanoparticle concentration for a fixed irradiation time of 40 ms. The kinetic of the diffusion process is indicated by the derivative of the time-dependent inflow in (c). A maximum inflow rate is achieved around 10 to 15 s. Connection of data points by smoothed lines solely serves for illustration purposes (Video 1 MP4, 7 MB [URL: http://dx.doi.org/10.1117/1.JBO.20.11.115005.1]).

(a)

(b)

Fig. 2 Kinetics of FM4-64 inflow in ZMTH3 cells after gold nanoparticle-mediated laser manipulation. (a) Sequence of images on a minute scale after the perforation event. A radiant exposure of 27 mJ/cm^2 and 0.5 μg/cm^2 gold nanoparticles were applied. Scale bar: 20 μm. (b) Corresponding normalized fluorescence values and applied fit functions. Directly after laser treatment, the signal is bleached by the manipulation laser (starting point below 0). Inflow of FM4-64 occurs in some cases over several minutes and goes into saturation (Video 2, MP4, 4 MB [URL: http://dx.doi.org/10.1117/1.JBO.20.11.115005.2]).

represents the phase of highest molecule exchange.[25,27] Additionally, this observation might be influenced by a possible accumulation of propidium iodide at the point of inflow in the cell.

We applied the dye FM4-64 to assess the membrane perforation over a time scale of minutes [Figs. 2(a) and 2(b) and Video 2]. FM4-64 has a similar weight to propidium iodide but binds to membraneous structures. In these experiments, fluorescence intensity was examined. The FM4-64 fluorescence bleached owing to the treatment laser pulse (please see laser control in Fig. 2) but increased due to FM4-64 inflow after perforation. The slope of the time dependence indicated a saturation of inflow.

The change of fluorescence could be well described by a diffusion model[35] for the concentration of FM4-64 in the cell: $C(t) = C_{max} \cdot \{1 - e^{[-t \cdot \ln(2)]/\tau}\}$—offset. The value C_{max}

represents the saturation of FM4-64 in the cell, τ describes the doubling time of the concentration, and the offset accounts for the laser-induced photobleaching.

Employing the method described above, we obtained values around 2.8 ± 0.3 min for τ by fitting this function to our data [Fig. 2(b) and Table 1]. This value is in agreement with previous studies by Yao et al. and Umebayashi et al. who analyzed propidium iodide uptake, added to the cell medium at various points in time after gold nanoparticle– or latex particle–mediated laser perforation. Uptake was observed up to several minutes after perforation.[36,37] Therefore, it is possible that the membrane remains permeable for small molecules, like ions, after perforation to rebalance cell homeostasis. Furthermore, the rearrangement of filamentous actin was observed within this time span.[27] Since the actin cortex is connected to the membrane, this could indicate membrane repair processes.
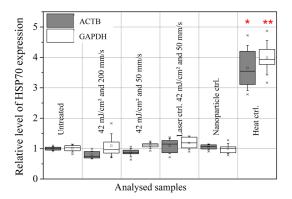
Table 1 Obtained fit values for the concentration doubling time.

Nanoparticle concentration (μg/cm^2)	Radiant exposure (mJ/cm^2)	Concentration doubling time τ (min)
0.05	15	2.6 ± 0.4
0.05	27	2.7 ± 0.2
0.05	41	2.6 ± 0.4
0.5	15	3.4 ± 0.6
0.5	27	2.9 ± 0.2
0.5	41	2.8 ± 0.2

3.2 Analysis of Cell Stress After Gold Nanoparticle–Mediated Laser Manipulation

The long-lasting membrane permeability also indicates that the cell might be affected by cell stress. Our previous observations on changes of area, volume, ion exchange, and cytoskeleton support this assumption.[27] To further analyze the cell response, we investigated the formation of ROS in the irradiated cells [Figs. 3(a) and 3(b)]. The fluorescence of DCF, a common indicator of ROS, was normalized to its initial value before treatment. It is challenging to evaluate ROS formation directly after laser treatment because this might also induce some radiant exposure dependent photobleaching. Therefore, a slight increase in fluorescence might be dominated by the bleaching or limited by the detection capabilities. An increase in fluorescence was clearly distinguishable from the background 5 min after

(a)   (b)

Fig. 3 Change of dichlorofluorescein (DCF) fluorescence in ZMTH3 cells after gold nanoparticle–mediated laser manipulation due to the additional formation of reactive oxygen species (ROS). (a) Sequence of microscopic images indicating the formation of ROS after perforation. A radiant exposure of 27 mJ/cm^2 and 0.5 μg/cm^2 gold nanoparticle were applied. Scale bar: 20 μm. (b) Increase in DCF fluorescence directly (0 min) and up to 11 min after perforation normalized to its initial value. Formation of ROS is highly dependent on the applied radiant exposures.
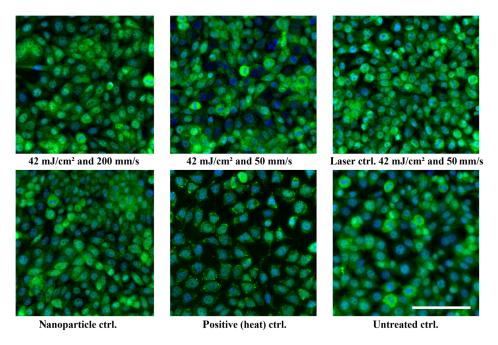
perforation for 41 mJ/cm^2 and at a later point in time for 27 mJ/cm^2 with a gold nanoparticle concentration of 0.5 μg/cm^2. The application of the lower gold nanoparticle concentration of 0.05 μg/cm^2 and laser irradiation without particles yielded fluorescence values in the same range as during the first 3 min in the 0.5 μg/cm^2 gold nanoparticle sample. As a consequence, we do not assume elevated levels of ROS in these samples and at these points in time. However, ROS formation might also be below our limit of detection in these cases. Additionally, at the points of perforation, possible dye outflow covered the signal of ROS formation at early points in time. The

observed fluorescence at later points in time indicates the formation of ROS and oxidative stress. These observations are in accordance with a previous study by Minai et al., who investigated the formation of ROS in cells at a fixed time in point of 90 min after femtosecond laser gold nanoparticle–mediated laser manipulation.[38] Our results indicate that the onset of the increased ROS formation occurs on a short time scale after perforation. However, it is questionable if there is a direct correlation between the membrane perforation event, for example, associated with lipid peroxidation, and the ROS formation or if endogenous ROS formation occurs as a cellular stress reaction. Based on the delayed response (5 min) in our observations, the latter appears more likely. A reason for increased endogenous ROS formation might be mitochondrial changes, which mainly release ROS into the cytoplasm. However, all regulatory levels and compartments of the cell might be involved in the ROS formation and redox signaling.[39]

The perforation process itself is connected to heating of the gold nanoparticles at the membrane. This heating process and further cellular stress events might induce the expression of heat shock proteins in the cell if certain cell stress levels are reached. In detail, cellular proteins might be thermally damaged during the manipulation process. Heat shock proteins prevent protein misfolding and aggregation during cell stress.[40,41] HSP70 is a well-understood HSP with a molecular mass of 70 kDa. In unstressed cells, it is bound to the heat shock factor 1 monomer (HSF1). Upon exposure to stress, HSF1 is released, undergoes trimerization, enters the nucleus, and is phosphorylated to induce the expression of HSP70 by binding in its gene promoter.[40,41] Maximum protein expression of HSP70 is accomplished in 3 to 5 h after the onset of cellular stress and is a reliable stress indicator.[41] Therefore, we analyzed HSP70 mRNA levels by RT-qPCR 2 h after laser treatment.

Fig. 4 Relative level of gene expression of HSP70 to the housekeeping genes ACTB and GAPDH determined by one-step quantitative real-time polymerase chain reaction analysis in ZMTH3 cells. In the positive control, heat treated 30 min at 45°C, a significant upregulation of HSP70 was detectable. Two laser-treated samples, a laser control, and a nanoparticle control showed no significant difference to the untreated control ($p > 0.38$). Gene expression levels were derived based on the $\Delta\Delta$CT method.

Fig. 5 Immunofluorescence staining of TIAR protein in L929 cells after gold nanoparticle–mediated laser manipulation. Cells were fixed 10 min after laser manipulation. In the overlays, cell nuclei are colored blue, and secondary antibody is in green. The formation of stress granules in the positive (heat) control (30 min at 45°C) is easily distinguishable from all other samples owing to the granularity. We did not observe stress granule formation in the laser-treated samples. Scale bar: 100 μm.

HSP70 expression was not upregulated in two laser-treated samples (42 mJ/cm^2 with 200/s and 50 mm/s scanning velocity) compared to an untreated control (see Fig. 4). Additionally, we did not observe any upregulation of gene expression in a laser control group, which was only laser irradiated but contained no nanoparticles, and in a nanoparticle control group. A conventionally heated control group showed a significant upregulation of HSP70 expression. During laser irradiation, particles are heated up several hundred degrees for a few 10 ns, while in the heat control, continuously heating until 45°C was applied over 30 min. The laser process is likely too short to induce significant protein activation and, thus, an elevation of HSP70 expression, although the marker also functions as a more general indicator of cell stress. Therefore, we conclude that a perforation with gold nanoparticle–mediated laser manipulation does not stimulate a cytoprotective effect through HSP70 expression for the applied laser parameters. The formation of oxidative stress is not necessarily connected to HSP expression, as long as proteins are not affected by the ROS formation.

To further extend our measurements of induced cell stress, we analyzed stress granule formation by immunofluorescence staining of the TIAR protein. Stress granules are composed of proteins and RNAs and are associated to translational arrest during cell stress.[42–45] Untranslated mRNAs accumulate in these granular structures after phosphorylation of the eukaryotic initiation factor eIF2a.[42] Aggregates of TIA-1 and TIAR are formed further downstream of this cascade and are required for stress granule assembly.[42,45] Stress granules are generally formed under various conditions of cell stress but, for example, not by treatment with hydrogen peroxide, actinomycin, lipopolysaccharides, and other specific cell stress inducers.[43] In the case of gold nanoparticle–mediated laser manipulation, stress granule formation was not observed by TIAR immunofluorescence staining in two laser-treated sample groups, the respective laser and nanoparticle controls, and in the untreated control at 10 min, 1 h, and 3 h after laser treatment (Fig. 5). In a heat-treated control group, granular structures in the cytoplasm served as evidence for stress granule formation.

As a consequence, gold nanoparticle–mediated laser manipulation does not seem to drive stress granule formation or the level of cell stress is not sufficient to initiate this process. These observations match our HSP70 expression measurements. A feedback regulation between stress granule formation and HSP70 prevents stress granules from aggregation owing to a modulation of the properties of TIA-1/TIAR by HSP70.[45] During HSP70 action upon stress, it is diverted away from TIA-1 such that stress granule assembly proceeds.[44]

4 Conclusion

Although many studies have proven the versatile applicability and efficacy of laser transfection procedures, only a few investigated the process-mediated consequences for single cells. In this study, we extended our previous work addressing cell volume, area, ion exchange, and filamentous actin (f-actin) cytoskeleton by an analysis of the perforation kinetics and the stress response in gold nanoparticle–mediated laser manipulation. The perforation kinetics indicates a sequential multistep procedure, which is supported by former calcium imaging and patch clamp analysis. Small molecules can penetrate the membrane even minutes after perforation. The initial time span possibly encompasses the inflow of larger molecules into the cell, whereas the later time span resembles the recovery of cellular homeostasis

and of the cell membrane. In this context, cell stress would be a potential disadvantage of gold nanoparticle–mediated laser manipulation. Although we showed the formation of ROS, neither heat stress nor the formation of stress granules was observed. The formation of ROS was dependent on the radiant exposure. In our previous study, changes in volume, area, calcium, and f-actin reorganization were also dependent on radiant exposure in a similar fashion. Endogenous ROS production and calcium transients are rapid cellular stress responses. ROS are involved in redox regulatory mechanisms, which could influence cellular homeostasis, maybe leading to cell death in some cases.[39]

As a conclusion, this study considerably extends our knowledge about laser-induced perforation and the associated biological processes, especially about the cellular response to the procedure.

References

1. M. Tsukakoshi et al., "A novel method of DNA transfection by laser microbeam cell surgery," *Appl. Phys. B* **35**, 135–140 (1984).
2. U. K. Tirlapur and K. König, "Targeted transfection by femtosecond laser," *Nature* **418**(6895), 290–291 (2002).
3. D. J. Stevenson et al., "Single cell optical transfection," *J. R. Soc. Interface* **7**(47), 863–871 (2010).
4. W. Tao et al., "Direct gene transfer into human cultured cells facilitated by laser micropuncture of the cell membrane," *Proc. Natl. Acad. Sci. U. S. A* **84**(12), 4180–4184 (1987).
5. Y. Shirahata et al., "New technique for gene transfection using laser irradiation," *J. Invest. Med.* **49**(2), 184–190 (2001).
6. G. Palumbo et al., "Targeted gene transfer in eucaryotic cells by dye-assisted laser optoporation," *J. Photochem. Photobiol. B.* **36**(1), 41–46 (1996).
7. G. Weber et al., "Genetic changes induced in higher plant cells by a laser microbeam," *Physiol. Plant.* **79**(1), 190–193 (1990).
8. N. Ma, F. Gunn-Moore, and K. Dholakia, "Optical transfection using an endoscope-like system," *J. Biomed. Opt.* **16**(2), 028002 (2011).
9. M. Antkowiak et al., "Application of dynamic diffractive optics for enhanced femtosecond laser based cell transfection," *J. Biophotonics* **3**(10–11), 696–705 (2010).
10. R. F. Marchington et al., "Optical injection of mammalian cells using a microfluidic platform," *Biomed. Opt. Express* **1**(2), 527–536 (2010).
11. F. Zanella, J. B. Lorens, and W. Link, "High content screening: seeing is believing," *Trends Biotechnol.* **28**(5), 237–245 (2010).
12. A. G. Doukas and T. J. Flotte, "Physical characteristics and biological effects of laser-induced stress waves," *Ultrasound Med. Biol.* **22**(2), 151–164 (1996).
13. D. J. McAuliffe et al., "Stress-wave-assisted transport through the plasma membrane in vitro," *Lasers Surg. Med.* **20**(2), 216–222 (1997).
14. J. S. Soughayer et al., "Characterization of cellular optoporation with distance," *Anal. Chem.* **72**(6), 1342–1347 (2000).
15. M. Ogura et al., "In vivo targeted gene transfer in skin by the use of laser-induced stress waves," *Lasers Surg. Med.* **34**(3), 242–248 (2004).
16. M. Terakawa et al., "Enhanced angiogenesis in grafted skins by laser-induced stress wave-assisted gene transfer of hepatocyte growth factor," *J. Biomed. Opt.* **12**(3), 034031 (2007).
17. Y.-C. Wu et al., "Massively parallel delivery of large cargo into mammalian cells with light pulses," *Nat. Methods* **12**, 439–444 (2015).
18. E. Boulais et al., "Plasmonics for pulsed-laser cell nanosurgery: fundamentals and applications," *J. Photochem. Photobiol. C Photochem. Rev.* **17**, 26–49 (2013).

19. G. Bisker and D. Yelin, "Noble-metal nanoparticles and short pulses for nanomanipulations: theoretical analysis," *J. Opt. Soc. Am. B* **29**(6), 1383 (2012).

20. J. Baumgart et al., "Off-resonance plasmonic enhanced femtosecond laser optoporation and transfection of cancer cells," *Biomaterials* **33**(7), 2345–2350 (2012).

21. D. Heinemann et al., "Gold nanoparticle mediated laser transfection for efficient siRNA mediated gene knock down," *PLoS One* **8**(3), e58604 (2013).

22. S. Kalies et al., "Immobilization of gold nanoparticles on cell culture surfaces for safe and enhanced gold nanoparticle-mediated laser transfection," *J. Biomed. Opt.* **19**(7), 070505 (2014).

23. M. Schomaker et al., "Characterization of nanoparticle mediated laser transfection by femtosecond laser pulses for applications in molecular medicine," *J. Nanobiotechnol.* **13**(1), 10 (2015).

24. S. Kalies et al., "Plasmonic laser treatment for Morpholino oligomer delivery in antisense applications," *J. Biophotonics* **7**(10), 825–833 (2014).

25. M. Schomaker et al., "Biophysical effects in off-resonant gold nanoparticle mediated (GNOME) laser transfection of cell lines, primary- and stem cells using fs laser pulses," *J. Biophotonics* **8**(8) 646–658 (2015).

26. S. Kalies et al., "Enhancement of extracellular molecule uptake in plasmonic laser perforation," *J. Biophotonics* **9**, 1–9 (2013).

27. S. Kalies et al., "Investigation of biophysical mechanisms in gold nanoparticle mediated laser manipulation of cells using a multimodal holographic and fluorescence imaging setup," *PLoS One* **10**(4), e0124052 (2015).

28. D. Heinemann et al., "Delivery of proteins to mammalian cells via gold nanoparticle mediated laser transfection," *Nanotechnology* **25**(24), 245101 (2014).

29. Z. Fan et al., "Spatiotemporally controlled single cell sonoporation," *Proc. Natl. Acad. Sci. U. S. A* **109**(41), 16486–16491 (2012).

30. C. A. Schneider, W. S. Rasband, and K. W. Eliceiri, "NIH Image to ImageJ: 25 years of image analysis," *Nat. Methods* **9**, 671–675 (2012).

31. A. Defour, S. C. Sreetama, and J. K. Jaiswal, "Imaging cell membrane injury and subcellular processes involved in repair," *J. Vis. Exp.* (85), e51106 (2014).

32. M. W. Pfaffl, G. W. Horgan, and L. Dempfle, "Relative expression software tool (REST) for group-wise comparison and statistical analysis of relative expression results in real-time PCR," *Nucleic Acids Res.* **30**(9), e36 (2002).

33. A. A. Davis et al., "Optoporation and genetic manipulation of cells using femtosecond laser pulses," *Biophys. J.* **105**(4), 862–871 (2013).

34. E. Casals et al., "Time evolution of the nanoparticle protein corona," *ACS Nano* **4**(7), 3623–3632 (2010).

35. L. Gu and S. K. Mohanty, "Targeted microinjection into cells and retina using optoporation," *J. Biomed. Opt.* **16**(12), 128003 (2011).

36. C. Yao et al., "Influence of laser parameters on nanoparticle-induced membrane permeabilization," *J. Biomed. Opt.* **14**(5), 054034 (2009).

37. Y. Umebayashi et al., "Elevation of plasma membrane permeability on laser irradiation of extracellular latex particles," *J. Biochem.* **134**(2), 219–224 (2003).

38. L. Minai, D. Yeheskely-Hayon, and D. Yelin, "High levels of reactive oxygen species in gold nanoparticle-targeted cancer cells following femtosecond pulse irradiation," *Sci. Rep.* **3**, 2146 (2013).

39. V. Adler et al., "Role of redox potential and reactive oxygen species in stress signaling," *Oncogene* **18**(45), 6104–6111 (1999).

40. M. G. Santoro, "Heat shock factors and the control of the stress response," *Biochem. Pharmacol.* **59**(1), 55–63 (2000).

41. J. G. Kiang and G. C. Tsokos, "Heat shock protein 70 kDa: molecular biology, biochemistry, and physiology," *Pharmacol. Ther.* **80**(2), 183–201 (1998).

42. N. Kedersha and P. Anderson, "Stress granules: sites of mRNA triage that regulate mRNA stability and translatability," *Biochem. Soc. Trans.* **30**(Pt 6), 963–969 (2002).

43. N. Kedersha and P. Anderson, "Mammalian stress granules and processing bodies," *Methods Enzymol.* **431**, 61–81 (2007).

44. P. Anderson and N. Kedersha, "Stress granules: the Tao of RNA triage," *Trends Biochem. Sci.* **33**(3), 141–150 (2008).

45. N. Gilks et al., "Stress granule assembly is mediated by prion-like aggregation of TIA-1," *Mol. Biol. Cell* **15**(12), 5383–5398 (2004).

Stefan Kalies is a graduate student at Hannover Biomedical Research School within the REBIRTH Cluster of Excellence, currently pursuing his PhD at the Laser Zentrum Hannover e.V. in the Department of Biomedical Optics. He studied physics at the Leibniz Universität Hannover. Currently he is working at Cornell University, US, for five months on laser transfection as a research stay during his PhD work.

Sebastian Keil obtained his bachelor's degree in biology from the Georg-August-University Göttingen. The project of his bachelor thesis was focused on the behavioral analysis of knockout mice lacking a protein that participates in myelination. He recently obtained his master's degree from the University of Veterinary Medicine Hannover, Germany. His master's thesis was dedicated to the investigation of the cellular response by gold nanoparticle–mediated laser manipulation, whose results are part of this paper.

Sina Sender is a master's student at the University of Veterinary Medicine Hannover, Germany, and is currently pursuing her master's thesis at the Laser Zentrum Hannover e.V. in the Department of Biomedical Optics. She received her BSc degree in biology from the Technical University Carolo-Wilhelmina zu Braunschweig, Germany, in 2013, and will receive her MSc in animal biology and biomedical sciences in 2015.

Susanne C. Hammer studied veterinary medicine at the University of Veterinary Medicine in Hannover, Germany. Since then, she has been working in the field of comparative oncology analyzing tumor-related gene expression as well as the establishment of tumor-derived cell lines.

Georgios C. Antonopoulos received his diploma in physics from RWTH Aachen University, Germany, in 2011. He then worked at the College of Optics and Photonics CREOL, University of Central Florida, Florida. Since 2012, he has been working as a PhD student at the Laser Zentrum Hannover e.V, Germany. His current research focuses both on experimental and numerical optics in the field of three-dimensional microscopy, optical tomography, and digital holography as applied to developmental and cell biology.

Markus Schomaker studied engineering science at the University of Applied Sciences Osnabrueck, Germany. He received his diploma in 2006 for his work with femtosecond laser and dental materials in co-operation with the dental hospital of the University of Frankfurt. Afterward, his PhD was about plasmonic laser perforation performed at Laser Zentrum Hannover e.V. Currently, he works as a postdoc at the Laser Components Department in Laser Zentrum Hannover e.V.

Tammo Ripken studied physics at the University of Hannover and received his PhD from the University of Hannover in 2007. Since 2001, he has worked at Laser Zentrum Hannover e.V. From 2005 to 2008, he was a project leader for femtosecond laser in ophthalmology. From 2008 to 2010, he led the Laser Medicine Group. Since 2010, he has acted as the head of the Biomedical Optics Department.

Hugo Murua Escobar studied biology at the University of Bremen, Germany. He worked in the field of human genetics, evaluating animal models for comparative oncologic approaches. Currently, his work aims at the identification and evaluation of cancer-related SNPs as well as expression changes.

Heiko Meyer studied applied laser technology at the University of Applied Sciences, Emden, and mechanical engineering at the Hanzehogeschool van Groningen. After receiving his diplomas in 2004, he started his PhD at IESL-FORTH in Crete and the Erasmus University Rotterdam, where he received his PhD in 2010. Since 2011, he has been working as a group leader for Biophotonic Imaging and Manipulation at Laser Zentrum Hannover e.V.

Dag Heinemann achieved his MSc in life science—cells and molecules at Leibniz University Hannover, Germany, in 2009. From 2009 to 2013, he passed on his PhD thesis concerning gold nanoparticle–mediated cell manipulation for biomedical approaches at Laser Zentrum Hannover e.V. Currently, he works as a postdoc at Laser Zentrum Hannover e.V. and is responsible for the research field of cytophotonics.